2nd International Conference "From Scientific Computing to Computational Engineering"
2nd IC-SCCE
Athens, 5-8 July, 2006

SOFT-TISSUE FLUID-STRUCTURE INTERACTIONS IN THE HUMAN BRAIN

Michalis A. Xenos*, MahadevaBharath R. Somayaji and **Andreas A. Linninger**
Laboratory for Product and Process Design
Departments of Chemical Engineering & Bioengineering, University of Illinois at Chicago,
Chicago IL, 60607
*e-mail: {xenos, linninge}@uic.edu

Keywords: cerebrospinal fluid (CSF); computational fluid dynamics; human brain, fluid-structure interaction

Abstract

Fluid-structure interaction (FSI) has important applications in biomedical engineering such as invasive drug delivery in the human brain, mechanics of fluid flow in distensible blood vessels and intracranial dynamics. Intracranial dynamics concerns the study of force interactions between soft tissues and fluid flows inside the brain. Many existing fluid-structure interaction approaches such as Immersed Boundary Method and Volume of Fluid do not satisfy conservation principles: conservation of mass and momentum and do not provide accurate resolution of the interfaces. This paper presents a physical and mathematical framework derived from first principles to solve a fluid-structure interaction (FSI) problem that satisfies both momentum and continuity balances and sharply tracks the interfaces between soft tissues and fluid.

The fluid and solid transport equations of mass and momentum are transformed into a moving, body-fitted reference frame. We present the motion of the conformal reference coordinate system using generalized curvilinear coordinates transformations. The proposed model accurately tracks the deformable interfaces between fluid and solid.

The equations describing fluid-structure interaction are coupled and consist of a nonlinear system of partial differential equations (PDEs). The governing PDEs are discretized using the finite volume method with both structured and unstructured meshes. Simultaneous solution approach using Newton-like methods was used instead of fixed-point iteration methods like SIMPLE algorithm due to strong coupling and inclusion of non-linear reactions terms in the governing equations. In addition, a comparison of the direct solutions approach against fixed-point iteration methods is provided.

1 INTRODUCTION

The brain is a complex organ composed of a porous parenchyma (gray and white matter) and fluids (CSF, blood). The CSF is contained in cavities within the brain, the ventricles, and in the subarachnoid space (SAS) that surrounds the brain. The CSF is produced in a pulsating manner from the choroid plexuses which are located on the walls of the ventricles. The ventricles are interconnected through the foramina and connected to the SAS through the foramina of Magendie and Luschke. The CSF is reabsorbed to venous blood through the arachnoid villi, located at the sagittal sinus [1]. A small portion of the CSF, two thirds of the constant production, seeps at each cardiac cycle from the porous brain parenchyma into the ventricular system. This seepage causes a pressure difference between the parenchyma and the lateral ventricles of the order of 1 mm Hg – transmural pressure [2]. The problems discussed in this study concern the understanding of intracranial dynamics and the mechanics of tissue deformation related to the enlargement of the brain ventricles and leading to a condition known as hydrocephalus. This pathological condition, affecting 70,000 people every year in US, causes symptoms such as headache, gait, dementia and if untreated may be fatal in both infants as well as adults [3].

Understanding intracranial dynamics. Abnormal CSF flow dynamics is responsible for a number of brain disorders [4], [5] but variations in intracranial pressure (ICP) and CSF flow patterns in the brain under pathological conditions such as hydrocephalus are still poorly understood. Despite numerous detailed studies on the pattern and timing of CSF motion with MRI techniques [6]-[8] the causes and mechanical principles underlying intracranial dynamics of hydrocephalus are still controversial. Early studies suggested that large ICP differences between the ventricles and the subarachnoidal space are responsible for the development of hydrocephalus [4]. However, more recent studies show that communicating hydrocephalus is inconsistent with large transmantle pressure differences [9], [10] and this result was also obtained with CFD approaches [11]-[13].

Complex geometry of human brain. This controversy is partially due to structural complexity of the human brain which is composed of porous tissue (gray and white matter) as well as fluid compartments (ventricles, subarachnoidal space, blood vessels). Most of the existing mathematical models studying the CSF flow consider a simplified one-dimensional motion of the fluid that interacts with the brain parenchyma [14]-[16]. Unfortunately, these models are inadequate to accurately quantify the intracranial dynamics of the cerebral

circulation since they do not address the complex structure of the human brain. Other studies that take into consideration the complex brain structure are limited to describing the flow in the narrow aqueduct of Sylvius [17], [18] or to apply relatively simple tank models [19]. Other CSF flow models are describing the brain as an electrical analogy [20]. For any work concerning the study of dynamics of CSF flow it is imperative to address the complexity of the brain structure and not oversimplify the problem. The complexity of the brain forces us to work with unstructured grids as the one constructed from a coronal section of a human brain depicted in Figure 1, because this is the only way to accurately represent its geometry.

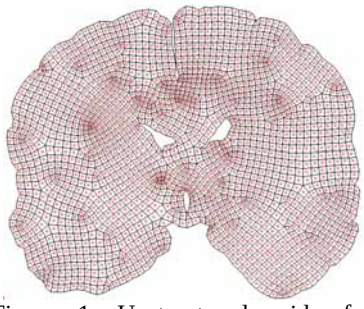

Figure 1. Unstructured grid of a coronal human brain section.

ICP measurements from fluid mechanics simulations. Magnetic Resonance Imaging (MRI) is a widely used, non-invasive method to characterize the CSF volumetric flow rate in normal and pathophysiological conditions. This analytical technique allows us to quantify the velocity field in vivo very accurately. However, this technique cannot provide information about the intracranial pressure (ICP), which is critical for the evaluation of the patient's status. Invasive techniques are required, involving the insertion of catheters in the brain [21]. We propose an alternative approach involving accurate MR measurements of the CSF flow field and the computational analysis of this flow by integrating MR images, image reconstruction tools and Computational Fluid Dynamics (CFD) software [12], [13].

The brain is a complex organ with gyrations and arbitrary boundaries. Therefore, it is imperative to develop a methodology that is applicable in domains with complex shapes. The application of generalized curvilinear coordinates (GCC) provides the ability to model complex structures such as the brain. Section 2 presents the fluid and solid transport equations of mass and momentum transformed into a moving, body-fitted coordinate system using GCC. Section 3 describes the discretization of equations using the finite volume method in structured meshes. The solution approach used is a direct approach based on the inexact Newton method instead of the fixed-point iteration methods such as SIMPLE algorithm. A comparison of the direct solutions approach against fixed-point iteration method is presented in section 3. Section 4 presents the quantification of cerebrospinal fluid (CSF) flow field in the brain and the deformation of soft tissues of the human brain under the influence of the pulsatile flow.

2 METHODOLOGY AND MATHEMATICAL FORMULATION

In this section we present the fundamental fluid and solid conservation laws. The governing equations for both phases are transformed to a moving, body-fitted coordinate system using the concept of generalized curvilinear coordinates (GCC) [22].

Mathematical formulation for the fluid equations in generalized coordinates. The governing equations (continuity and Navier-Stokes equations) in Cartesian coordinates for a two-dimensional, Newtonian and incompressible fluid can be written in dimensional form as:

$$\frac{\partial \rho}{\partial t}+\frac{\partial(\rho u)}{\partial x}+\frac{\partial(\rho v)}{\partial y}=0 \tag{1}$$

$$\rho\left(\frac{\partial u}{\partial t}+\frac{\partial(uu)}{\partial x}+\frac{\partial(uv)}{\partial y}\right)=-\frac{\partial p}{\partial x}+\frac{\partial}{\partial x}\left(\mu\frac{\partial u}{\partial x}\right)+\frac{\partial}{\partial y}\left(\mu\frac{\partial u}{\partial y}\right) \tag{2}$$

$$\rho\left(\frac{\partial v}{\partial t}+\frac{\partial(uv)}{\partial x}+\frac{\partial(vv)}{\partial y}\right)=-\frac{\partial p}{\partial y}+\frac{\partial}{\partial x}\left(\mu\frac{\partial v}{\partial x}\right)+\frac{\partial}{\partial y}\left(\mu\frac{\partial v}{\partial y}\right) \tag{3}$$

It is advantageous to build a sharp interface tracking method for moving objects or phase boundaries by expressing the motion of both phases (fluid and solid) with the help of an Eulerian-Langrangian technique. Early researchers proposed mathematical relations for temporal changes of a transport property within "moving" reference frames [23], [24]. We implemented such a body-fitted moving grid by extending the generalized curvilinear transformation as depicted in Figure 2. Using the Eulerian-Langrangian approach, the continuity and momentum equations in Cartesian coordinates, Eqs. (1)-(3), can be transformed in a moving body-fitted approach [23]. In two-dimensions, the continuity and fluid transport equations in curvilinear coordinates ($\xi=\xi(x,y,t)$, $\eta=\eta(x,y,t)$) for an incompressible fluid in a moving frame can be written as in Eqs. (4)-(6):

$$\frac{\partial(J\rho)}{\partial t}+\frac{\partial(\rho U)}{\partial \xi}+\frac{\partial(\rho V)}{\partial \eta}=0 \tag{4}$$

$$\rho\left(\frac{\partial(Ju)}{\partial t}+\frac{\partial(Uu)}{\partial \xi}+\frac{\partial(Vu)}{\partial \eta}\right)=-\left(y_\eta\frac{\partial p}{\partial \xi}-y_\xi\frac{\partial p}{\partial \eta}\right)+\frac{\partial}{\partial \xi}\left[\frac{\mu}{J}\left(q_1u_\xi-q_2u_\eta\right)\right]+\frac{\partial}{\partial \eta}\left[\frac{\mu}{J}\left(q_3u_\eta-q_2u_\xi\right)\right] \tag{5}$$

$$\rho\left(\frac{\partial(Jv)}{\partial t}+\frac{\partial(Uv)}{\partial\xi}+\frac{\partial(Vv)}{\partial\eta}\right)=-\left(x_\xi\frac{\partial p}{\partial\eta}-x_\eta\frac{\partial p}{\partial\xi}\right)+\frac{\partial}{\partial\xi}\left[\frac{\mu}{J}\left(q_1v_\xi-q_2v_\eta\right)\right]+\frac{\partial}{\partial\eta}\left[\frac{\mu}{J}\left(q_3v_\eta-q_2v_\xi\right)\right] \tag{6}$$

Here *u*, *v* are the components of the velocity vector of the fluid, *p* the static pressure of the fluid, $x_\xi, x_\eta, y_\xi, y_\eta$ are the metrics of the transformation, J is the determinant of the inverse Jacobian of the transformation from the physical moving domain to the normalized reference domain (Eq. (7)), $q_1 = x_\eta^2 + y_\eta^2$, $q_2 = x_\xi x_\eta + y_\xi y_\eta$ and $q_3 = x_\xi^2 + y_\xi^2$. U, V are the contra-variant velocity components as defined in Eq. (7) and μ is the viscosity of the fluid.

If we adjust the grid movement to accurately track the interface between solid tissue and fluid flow, the fluid and solid phase are separated sharply even when their interface boundary is moving. The arbitrary "Eulerian-Langrangian" grid motion is made possible by considering the Jacobian of the transformation, *J(t)*, as a function of time and the transformed (contra-variant) velocities as a function of the current physical *u*, *v* velocities of the fluid and the velocities of the grid motion, $\dot{x}$, $\dot{y}$.

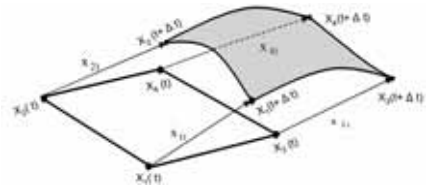

Figure 2. Moving reference frame

$$\begin{aligned} U &= (u-\dot{x})\,y_\eta-(v-\dot{y})\,x_\eta,\\ V &= (v-\dot{y})\,x_\xi-(u-\dot{x})\,y_\xi.\\ J &= \frac{\partial x}{\partial\xi}\frac{\partial y}{\partial\eta}-\frac{\partial x}{\partial\eta}\frac{\partial y}{\partial\xi}. \end{aligned} \tag{7}$$

Eqs. (4)-(6) describe the motion of a fluid in a complex geometry that can arbitrarily change its shape and this is possible with the introduction of the above described formulation. In the next subsection we will present the constitutive equations that describe the displacement of a linear elastic body of an arbitrary shape. The coupling of the fluid and solid equations in generalized coordinates will help us to solve problems describing the interaction of fluid and solid phases.

Mathematical formulation for the solid equations in generalized coordinates. The governing equations (Newton's Law and incompressibility condition) in Cartesian coordinates for a two-dimensional, linear elastic incompressible isotropic solid can be written in dimensional form as:

$$\rho_s\frac{\partial^2\alpha}{\partial t^2}=-\frac{\partial\Omega}{\partial x}+G\left(\frac{\partial^2\alpha}{\partial x^2}+\frac{\partial^2\alpha}{\partial y^2}\right)+G\left(\frac{\partial^2\alpha}{\partial x^2}+\frac{\partial^2\beta}{\partial y\partial x}\right)+F_x, \tag{8}$$

$$\rho_s\frac{\partial^2\beta}{\partial t^2}=-\frac{\partial\Omega}{\partial y}+G\left(\frac{\partial^2\beta}{\partial x^2}+\frac{\partial^2\beta}{\partial y^2}\right)+G\left(\frac{\partial^2\alpha}{\partial x\partial y}+\frac{\partial^2\beta}{\partial y^2}\right)+F_y, \tag{9}$$

$$\frac{\partial\alpha}{\partial x}+\frac{\partial\beta}{\partial y}=0, \tag{10}$$

where α, β are the displacements in *x* and *y* directions and *G* is the shear modulus ($G = \nu E/2(1+\nu)$, where *E* is the Young modulus and *v* is Poisson's ratio). If we consider the brain parenchyma as an incompressible material we have to take under consideration that $\vec{\nabla}\cdot\vec{q}=0$ (where $\vec{q}$ is the vector of displacement) and to replace the term $(\lambda+G)\vec{\nabla}(\vec{\nabla}\cdot\vec{q})$ by $-\vec{\nabla}\Omega$ [25]. The term $\vec{\nabla}\cdot\vec{q}=0$ means that the volume remains the same as the shape of the elastic body changes; this implies that the Poisson's ratio (*v*) remains constant and equal to 0.5. In order to evaluate stresses and strains we will use the relations shown below that combine stresses with strains and displacements.

$$\sigma_x=-\Omega+2G\,\varepsilon_x=-\Omega+2G\frac{\partial\alpha}{\partial x}, \tag{11}$$

$$\sigma_y=-\Omega+2G\,\varepsilon_y=-\Omega+2G\frac{\partial\beta}{\partial y}, \tag{12}$$

$$\tau_{xy}=G\gamma_{xy}=G\left(\frac{\partial\alpha}{\partial y}+\frac{\partial\beta}{\partial x}\right). \tag{13}$$

Where σ_x is the normal stress in *x*-direction σ_y is the normal stress in *y*-direction and τ_{xy} is the shear stress. The system of equations for the linear elastic solid is written in generalized coordinates as:

$$\rho_s \frac{\partial^2 (J\alpha)}{\partial t^2} = -\left(y_\eta \frac{\partial \Omega}{\partial \xi} - y_\xi \frac{\partial \Omega}{\partial \eta} \right) + 2G \frac{\partial}{\partial \xi}\left(\frac{q_1}{J}\alpha_\xi - \frac{q_2}{J}\alpha_\eta \right) + G \frac{\partial}{\partial \eta}\left(\frac{q_3}{J}\alpha_\eta - \frac{q_2}{J}\alpha_\xi \right) + G\left(-\frac{\partial}{\partial \xi}\left(\frac{x_\eta y_\eta}{J}\beta_\xi \right) + \frac{\partial}{\partial \xi}\left(\frac{x_\eta y_\xi}{J}\beta_\eta \right) + \frac{\partial}{\partial \eta}\left(\frac{x_\xi y_\eta}{J}\beta_\xi \right) - \frac{\partial}{\partial \eta}\left(\frac{x_\xi y_\xi}{J}\beta_\eta \right) \right) + JF_x, \quad (14)$$

$$\rho_s \frac{\partial^2 (J\beta)}{\partial t^2} = -\left(x_\xi \frac{\partial \Omega}{\partial \eta} - x_\eta \frac{\partial \Omega}{\partial \xi} \right) + 2G \frac{\partial}{\partial \xi}\left(\frac{q_1}{J}\beta_\xi - \frac{q_2}{J}\beta_\eta \right) + G \frac{\partial}{\partial \eta}\left(\frac{q_3}{J}\beta_\eta - \frac{q_2}{J}\beta_\xi \right) + G\left(-\frac{\partial}{\partial \xi}\left(\frac{x_\eta y_\eta}{J}\alpha_\xi \right) + \frac{\partial}{\partial \xi}\left(\frac{x_\xi y_\eta}{J}\alpha_\eta \right) + \frac{\partial}{\partial \eta}\left(\frac{x_\eta y_\xi}{J}\alpha_\xi \right) - \frac{\partial}{\partial \eta}\left(\frac{x_\xi y_\xi}{J}\alpha_\eta \right) \right) + JF_y, \quad (15)$$

$$\frac{\partial \left(\rho_s (y_\eta \alpha - x_\eta \beta) \right)}{\partial \xi} + \frac{\partial \left(\rho_s (x_\xi \beta - y_\xi \alpha) \right)}{\partial \eta} = 0, \quad (16)$$

Eqs. (14)-(16) describe the displacements of a two-dimensional linear elastic body with an arbitrary geometry. These solid equations are to be coupled with the fluid flow (e.g. blood or CSF) by kinematic and force boundary conditions that will be described further. Specifying appropriate boundary conditions at the interface between fluid and solid we can predict the displacement and stress fields that the solid experiences under the influence of the fluid. The appropriate boundary conditions for the fluid-solid interaction are presented in the next subsection.

Boundary conditions of the problem. At the lower structure (AFEB), an incompressible viscous and Newtonian fluid is flowing and the boundary conditions for the fluid are shown in Figure 3 (bottom). More precisely, at the Inflow (AB), we impose a time dependent condition $u_{\text{in}}(t) = a(1.0 + 0.5\sin(2\pi t))$ that describes the pulsatile motion of the blood into the vessels or the CSF in the ventricles of the human brain. The wall (AF) is rigid and we impose no slip boundary condition ($u = v = 0$). The wall (BE) is flexible and we impose that the fluid velocity is equal to the velocity of the surface ($u = u_{surface}, v = v_{surface}$). Finally for the outflow (FE) we impose zero derivatives, $\partial u/\partial x = \partial v/\partial x = 0$ meaning that the velocity of the fluid has obtained the parabolic profile.

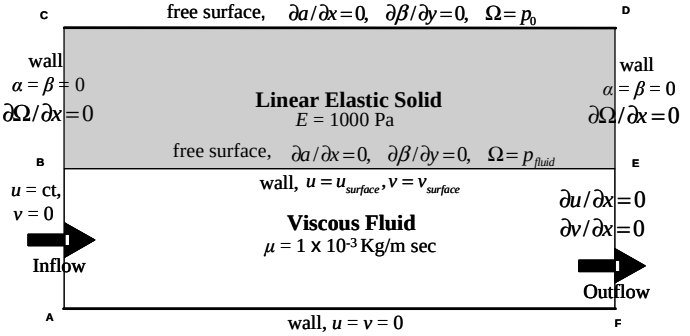

Figure 3. Boundary conditions of the problem

At the upper structure (BEDC) we consider a linear elastic and incompressible solid, the boundary conditions for the solid structure are shown in Figure 3 (top). More precisely, at the left (CB) and right (ED) boundary surfaces of the solid we impose a wall boundary condition for the solid, namely the displacements are zero at these surfaces $(\alpha = \beta = 0)$ and the pressure remains constant on the wall $(\partial\Omega/\partial x = 0)$. On the other two surfaces we impose a free surface boundary conditions, namely the normal stresses (σ_x, σ_y) on the surfaces has to be zero, this boils down to the imposed boundary conditions, $(\varepsilon_x = \partial\alpha/\partial x = 0,\ \varepsilon_y = \partial\beta/\partial y = 0, \Omega = p_{out})$.

3 NUMERICAL SOLUTION

Finite volume discretization in curvilinear coordinates. When using Finite Differences or Finite Volumes methods to calculate partial derivatives it would be natural to place all state variables (*p*, *u*, *v*, *ρ*, *T*, etc.) in an equidistant grid, represent all variables on the grid points, and then use centered differences as an approximation to the derivatives. Unfortunately this approach does not work well especially in convective dominated flows ($Peclet = (\rho u L/\mu) >> 1$. A common solution to this is using a staggered grid approach [26]. This means that instead of placing all variables in one grid, different variables are placed on different grids, which are shifted half a grid point. On this stagger grid we use differential operators that return the result shifted half a point up or down along the grid. These operators use adjacent grid points instead of alternate grid points.

In our approach a grid system is generated numerically at the positions marked with triangles. The scalar variables (*p*, *ρ*, *k* etc.) are located in the arithmetic center of the four adjacent grids marked by the circle. Both *u* and *U* are located at the midpoint of the *east* and *west* faces of the control volume. Both *v* and *V* are located at the midpoint of the *north* and *south* faces of the control volume (Figure 4). For a typical grid node *P* the finite-difference approximation to the conservation laws (*x*, *y*-momentum, continuity, etc.) can be performed by taking the integral of the equation (Eqs. (4)-(6) and (14)-(16)) over the control volume and discretizing it [23], [24].

The upwind scheme is also introduced to our formulation in order to overcome problems concerning the high convection terms in the momentum equations. With this formulation we minimize the influence of the convection terms retaining the diffusion terms unchanged as the velocity increases in the flow field. For the convection terms we have to make some assumptions, discretizing them with first order accuracy instead of the second order that the diffusion terms will retain. When the local velocity gradients are large the solution is inaccurate. More accurate solution is obtained if higher order upwind scheme are utilized [27] or with the use of the power law scheme [26].

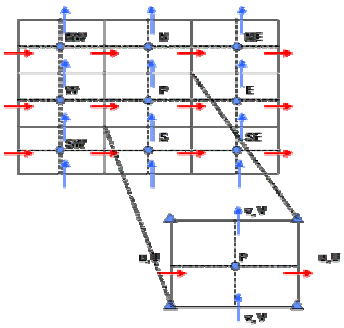

Figure 4. Configuration of a stagger grid

If an analytical relationship for converting the (x,y) domain into the (ξ,η) domain does not exist, we can use the concept of the approximate metrics of the transformation as shown in Eq. (17). We use finite differences to describe the metrics of the transformation for a point P (Figure 5) using a centered difference evaluation [27]:

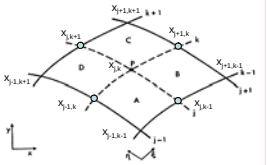

Figure 5. Equivalent computational grid in the physical domain

$$x_\xi = \frac{\partial x}{\partial \xi} \approx \frac{x_{j+1,k} - x_{j-1,k}}{\Delta \xi}, \quad x_\eta = \frac{\partial x}{\partial \eta} \approx \frac{x_{j,k+1} - x_{j,k-1}}{\Delta \eta}$$
$$y_\xi = \frac{\partial y}{\partial \xi} \approx \frac{y_{j+1,k} - y_{j-1,k}}{\Delta \xi}, \quad y_\eta = \frac{\partial y}{\partial \eta} \approx \frac{y_{j,k+1} - y_{j,k-1}}{\Delta \eta} \tag{17}$$

Accordingly, the determinant of the inverse Jacobian of the transformation becomes:

$$\det J^{-1} = \left| J^{-1} \right| = x_\xi y_\eta - x_\eta y_\xi = \frac{x_{j+1,k} - x_{j-1,k}}{\Delta \xi} \frac{y_{j,k+1} - y_{j,k-1}}{\Delta \eta} - \frac{x_{j,k+1} - x_{j,k-1}}{\Delta \eta} \frac{y_{j+1,k} - y_{j-1,k}}{\Delta \xi}. \tag{18}$$

Without loss of generality we arbitrarily choose $\Delta \xi = \Delta \eta = 1$ [23] (the size of the generalized grid), a uniform grid is assumed for (ξ,η).

Direct and Iterative solution approaches to Navier-Stokes Equations. Many problems in transport processes and fluid dynamics require solution of a coupled system in which the dominant variable of each equation occurs in other equations too (momentum and continuity). In the simultaneous approach, all equations are considered part of a single system and the discretized equations have a block-banded structure [28]. Solving a multidimensional problem on a very fine grid with governing equations that are non-linear, using direct solution of these equations would be expensive and time consuming. In addition, the computational effort involved for the calculation of Jacobians (N^3 x N^3) is expensive especially when the discretization is too fine. However, when the governing equations are non-linear and tightly coupled, the direct solution approach would be the best solution strategy.

For solving non-linear equations, non-linear solvers like Newton-like methods and global methods can be used. The path to a solution will depend on good initial guess values and the actual path to the solution. Newton-like methods are much faster with a good initial guess and with a good estimate of the solution but may suffer from local minima. Global methods are more robust and offer security for convergence. There exists a trade-off in using local and global methods.

Iterative methods employ a guess-correct philosophy that gradually improves the guessed solution by repeated use of the discrete governing equations. The governing partial differential equations in fluid dynamics tend to be solved iteratively [29], [30]. When the governing equations are non-linear, it is preferable to treat each equation considering it to have one unknown, temporarily treating other variables as known using the current values. For instance, SIMPLE like methods approximate to Gauss-Siedel method in which the unknowns (velocity and pressure correction) are solved sequentially. In semi-implicit methods, is hard to analyze the convergence of these methods and the selection of under relaxation factors is specific to the system being analyzed [28]. In contrast to the simultaneous approach, the calculation of the Jacobians (N x N) required for each sub-system is not so expensive when using a non-linear solver thus making the method convenient to use for very fine grid sizes. Figure 6 illustrates the time that the direct solution approach and the fixed-point iteration methodology need to converge to the solution for the same grid volumes. It can be observed that the direct solution approach converges faster for small number of grid volumes but as the size of the grid increases the computational time increases exponentially. On the other hand, the solution of the fixed-point iteration method converges slower than the direct methodology for smaller grids.

In the proposed methodology, we are solving the linear subsystem of equations simultaneously by applying a direct numerical approach as described in the previous paragraphs. In order to solve the non-linear system of equations specifically developed solver algorithms based on inexact Newton method and high-speed sparse matrix solution techniques are used [31], [32]. We have refined these techniques for the solution of large-scale systems of algebraic equations in a reasonable amount of time. The current developed methodology is using the finite volume method in generalized curvilinear coordinates in both fluids and solids. This approach makes the numerical solution of the system easier especially due to the fact that no special interpolation is needed at the interface between the two media. Finally the conservation of mass and momentum for both phases is satisfied at least to the power of the accuracy of the solver. In the next section we present results that illustrate the described fluid-structure interaction methodology. These results provide the proof of concept that our approach is applicable to biomedical applications as the interactions of soft brain tissues with the pulsating CSF.

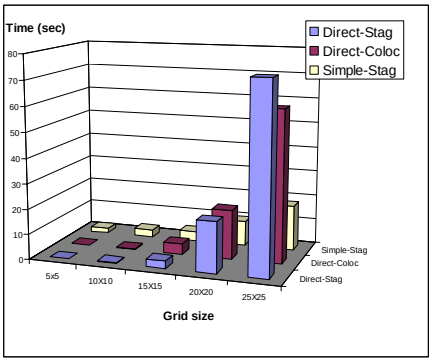

Figure 6. Comparison of direct solution approach vs. the iterative solution approach (SIMPLE).

4 RESULTS AND DISCUSSION

In this study we present two-dimensional results from the fluid-structure interaction model that can describe the interaction of soft tissue (brain parenchyma) with viscous fluid (CSF, blood). The quantities that usually are studied in fluid-solid interactions are the velocity of the fluid, the displacement of the solid structure and the pressure in both media. In this study we will also present results that concern normal and shear stresses on the two phases due to the motion of the fluid.

Fluid-structure interaction on a simple geometry. Figure 7 displays the two-dimensional velocity field for the fluid (bottom) and the displacement for the solid (top) at four different time steps during the cardiac cycle (1 sec). The pressure field for the viscous fluid and the linear elastic body is also presented in Figure 7 at four

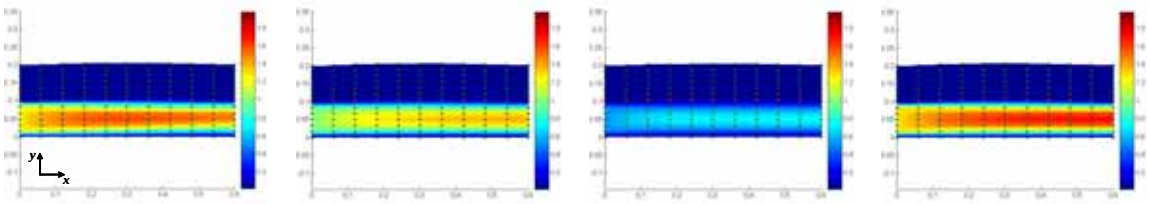

Velocity field, t = 0.1 sec Velocity field, t = 0.4 sec Velocity field, t = 0.7 sec Velocity field, t = 1.0 sec

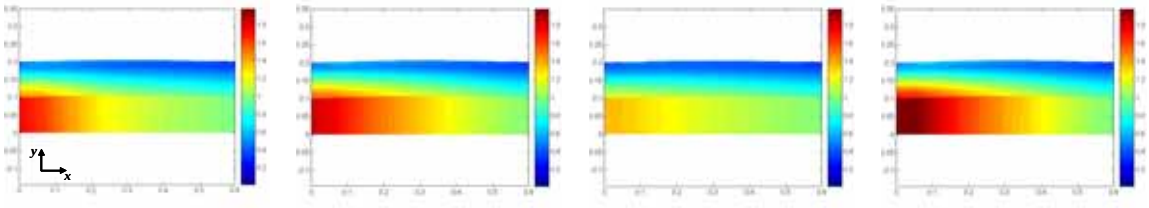

Pressure field, t = 0.1 sec Pressure field, t = 0.4 sec Pressure field, t = 0.7 sec Pressure field, t = 1.0 sec

Figure 7. Interactions of fluid and solid over a period of 1sec

different time steps during the cardiac cycle (1 sec). It is observed that as the inflow velocity of the fluid increases the solid displacement increases. The inflow velocity is considered as a plug flow and due to viscous forces the flow obtains the parabolic profile after a small distance from the inflow. The highest displacement of the solid occurs in the center of the media due to the fact that the solid cannot be displaced near the fixed walls (see boundary conditions).The pressure field in the fluid is higher at the inflow and an almost linear pressure drop occurs throughout the fluid. The solid experiences this pressure drop and the highest pressure in the solid structure occurs near the free surface that it is in immediate interaction with the fluid near the fluid inflow. The pressure in the linear elastic body exhibits a drop in the *y*-direction, with highest pressure at the interface with the fluid and lower at the top free surface.

Figure 8 displays the stresses acting on fluid and solid structure at the peak velocity of the fluid occurring at t = 0.2 sec. It is observed that the highest normal stresses occur near the inflow of the fluid for both structures,

solid and fluid. The highest shearing stresses occur near the wall for the solid structure because the solid is fixed on the wall and cannot experience a motion.

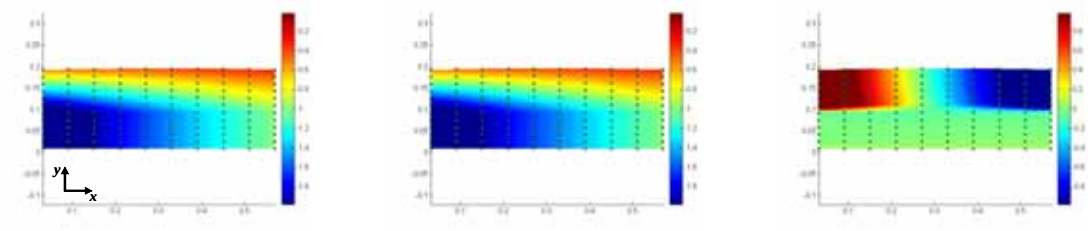

σ_x stress field for t = 0.2 sec σ_y stress fields for t = 0.2 sec τ_{xy} stress fields for t = 0.2 sec

Figure 8. Stress field for fluid and solid at the peak of the velocity.

Unstructured grids for the human brain. In the previous subsection, we presented the proof-of-concept for the developed FSI methodology on simplified geometry using structured grids. A future step would be to apply the developed mathematical FSI model to complex human brain structures constructed with unstructured grids. We have already modeled the complex structures of the human brain that include the ventricular system, the subarachnoid space (SAS) and the parenchyma using static unstructured grids [13]. Figure 9 illustrates the velocity field of the CSF in the ventricular and SAS structures on static unstructured grids. In these simulations, we were able to predict velocities very close to experimental MRI velocities and predict the pressure field, which is very difficult to be obtained otherwise non-invasively. Future directions include the application of the FSI model on these unstructured grids and the consistent representation of the human brain physiology and quantification of the soft brain tissues interactions with the biological fluids (CSF, blood).

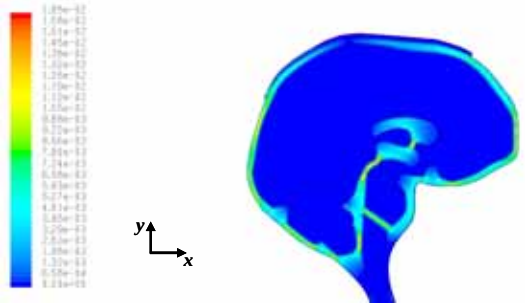

Figure 9. Two-dimensional velocity magnitude for a normal brain on unstructured grids at the peak of the pulsatile CSF velocity.

Closing the presentation of the fluid-structure interaction model, we summarize the most important findings from the mathematical analysis and the advantages of the proposed model for the prediction of pathophysiological conditions without use of invasive techniques. The application of first principles models of fluid and solid mechanics provides the medical community with a computational tool to quantify tissue displacements in normal and pathological conditions in the human brain.

5 CONCLUSIONS

- A two-dimensional fluid-solid interaction model was presented for the prediction of the fluid-tissue interactions in normal and pathological conditions (hydrocephalus).
- The proposed model can accurately predict the velocity field of the fluid, the total displacement of the solid and the pressure field in both phases (fluid and solid).
- The extraction of normal and shearing stresses provide information for the forces acting on both structures.
- This model gives the opportunity to design new treatments and predict pathologies without the need of in vivo testing of the patients.

References

[1] Kandel, E., Schwartz, J.H., Jessell, T.M., (1991), *Principles of Neural Science*, 3rd ed., Appleton & Lange, New York.

[2] Smith, J.J., Kampine, J.P., (1984), *Circulatory Physiology – the essentials*, 2nd ed., Williams & Wilkins, Baltimore.

[3] McLone, D.G., (2001), *Pediatric neurosurgery, surgery of the developing nervous system*, Philadelphia, Saunders.

[4] Hakim, S., Venegas, J.G. and Burton, J.D., (1976), "The physics of the cranial cavity, hydrocephalus and normal pressure hydrocephalus: mechanical interpretation and mathematical model", Surg. Neurol., Vol. 5, pp. 187-210.

[5] Nagashima, T., Horwitz, B., Rapoport, S.I., (1990), "A mathematical model for vasogenic brain edema", Advances in neurology, Vol. 52, pp. 317-326.

[6] Enzmann, D.R., Pelc, N.J., (1992), "Brain motion: measurement with phase-contrast MR imaging", Radiology, Vol. 185, No. 3, pp. 653-660.

[7] Greitz, D., Franck, A., Nordell, B., (1993), "On the pulsatile nature of intracranial and spinal CSF – circulation demonstrated by MR Imaging", Acta Radiologica, Vol. 34, pp. 321-328.
[8] Zhu, D.C., Xenos, M., Linninger A.A., and Penn, R.D., (accepted, 2006), "Dynamics of Lateral Ventricle and Cerebrospinal Fluid in Normal and Hydrocephalic Brains", Journal of Magnetic Resonance Imaging.
[9] Penn, R.D., Lee, M.C., Linninger, A.A., Miesel, K., Lu, S.N., Stylos, L., (2005), "Pressure Gradients in the Brain: an Experimental Model of Hydrocephalus", J. Neurosurgery, Vol. 102, pp. 1069-1075.
[10] Stephensen, H., Tisell, M., Wikkelso, C., (2002), "There is no transmantle pressure gradient in communicating or noncommunicating hydrocephalus", Neurosurgery, Vol. 50, No. 4, pp. 763-771.
[11] Linninger, A.A., Tsakiris, C., Zhu, D.C., Xenos, M., Roycewicz, P., Danziger, Z., Penn, R., (2005), "Pulsatile cerebrospinal fluid dynamics in the human brain", IEEE Transactions on Biomedical Engineering Vol. 52, No. 4, pp. 557-565.
[12] Xenos, M., and Linninger, A.A., (2004), "Large-scale fluid structure interaction modeling in the human brain", AIChE Annual Meeting, November 7-12, Austin, TX.
[13] Linninger, A.A., Xenos, M., Zhu, D., Somayaji, M.B.R., Kondapalli, S., and Penn, R. (submitted, 2006), **"**Cerebrospinal Fluid Flow in the Normal and Hydrocephalic Human Brain", IEEE Transactions on Biomedical Engineering.
[14] Levine D.N., (1999), "The pathogenesis of normal pressure hydrocephalus: a theoretical study", Bulletin of mathematical biology, Vol. 61, pp. 875-916.
[15] Sivaloganathan, S., Tenti, G., Drake, J.M., (1998), "Mathematical pressure volume models of the cerebrospinal fluid. Applied Mathematics and Computation", Vol. 94, pp. 243-266.
[16] Ursino, M., Gimmarco, D.P., (1991), "A Mathematical Model of the Relationship between Cerebral Blood Volume and Intracranial Pressure Changes: The Generation of Pleatue Waves", Annals of Biomedical Engineering, Vol. 19, pp. 15-42.
[17] Fin, L., and Grebe, R., (2003), "Three Dimensional Modeling of the Cerebrospinal Fluid Dynamics and Brain Interactions in the Aqueduct of Sylvius", Computer Methods in Biomechanics and Biomedical Engineering, Vol. 6, No. 3, pp. 163-170.
[18] Jacobson, E.E., Fletcher, D.F., Morgan, M.K., and Johnston, I.H., (1996), "Fluid Dynamics of the Cerebral Aqueduct", Pediatr. Neurosurg., Vol. 24, pp. 229-236.
[19] Ammourah, S., Aroussi, A., and Vloberghs, M., (2003), "Cerebrospinal Fluid dynamics in a Simplified Model of the Human Ventricular System", 11th Annual Conference on CFD 2003, Vancouver BC, Canada, May 28-30.
[20] Egnor, M., Zheng, L., Rosiello, A., Gutman, F., Davis, R., (2002), "A model of pulsations in communicating hydrocephalus", Pediatr Neurosurg., Vol. 36, pp. 281-303.
[21] Raksin, P.B., Alperin, N., Sivaramakrishnan, A., Surapaneni, S., and Lichtor, T., (2003), "Noninvasive intracranial compliance and pressure based on dynamic magnetic resonance imaging of blood flow and cerebrospinal fluid flow: review of principles, implementation, and other noninvasive approaches", Neurosurg Focus, Vol. 14, No. 4, pp. 1-8.
[22] Thompson, J.F., Warsi, Z.U.A., Mastin, C.W., (1985), *Numerical Grid Generations, Foundations and Applications*, North-Holland, New York.
[23] Shyy, W., Tong, S.S., and Correa, S.M., (1985), "Numerical recirculating flow calculation using a body-fitted coordinate system", Numerical Heat Transfer, Vol. 8, pp. 99-113.
[24] Braaten, M., and Shyy, W., (1986), "A study of recalculating flow computation using body-fitted coordinates: consistency aspects and mesh skewness", Numerical Heat Transfer, Vol. 9, pp. 559-574.
[25] Love, A.E.H., (1944), *A treatise on the mathematical theory of elasticity*, 4th ed., New York: Dover Publications.
[26] Patankar, S.V., (1980), *Numerical heat transfer and fluid flow*, McGraw-Hill, New York.
[27] Fletcher, C.A.J., (1991), *Computational Techniques for Fluid Dynamic*, Volume II, 2nd ed., Springer Verlag, Berlin.
[28] Ferziger, J.H., Peric, M., (2002), *Computational Methods for Fluid Dynamic*s, Springer-Verlag, 3rd ed., New York.
[29] Patankar, S., and Spalding, D., (1972), "A calculation procedure for heat, mass and momentum transfer in three-dimensional parabolic flows", Int. J. Heat Mass Transfer, Vol. 15, pp. 1787- 1807.
[30] Vandoormaal, J.P., Raithby, G.D., (1984), "Enhancements of the Simple Method for Predicting Incompressible Fluid-Flows", Numerical Heat Transfer, Vol. 7, pp. 147-163.
[31] Chowdry, S., and Linninger, A.A., (2001), "Automatic Structure Analysis of Large Scale Differential Algebraic Systems", Proc. IEEE Instrumentation and Measurement Technology Conference, Budapest,P1-7.
[32] Bahl, V., and Linninger, A.A., (2001), "Modeling of Event-Driven Continuous-Discrete Processes", Lecture Notes in Computer Science 2034, Springer Verlag, pp. 387- 402, ISBN 3-540-41866-0.